
BENCHMARKING PERFORMANCE, EXPLAINABILITY, AND EVALUATION STRATEGIES OF VISION-LANGUAGE MODELS FOR SURGERY: CHALLENGES AND OPPORTUNITIES

Jiajun Cheng¹, Xianwu Zhao¹, Shan Lin¹

¹School of Electrical, Computer, and Energy Engineering, Arizona State University
{ccheng58, xzhao183, shan.lin.2}@asu.edu

ABSTRACT

Minimally invasive surgery presents significant visual challenges, including a limited field of view, specular reflections, and inconsistent lighting conditions due to the small incision and use of endoscopes. Over the past decade, while many machine learning and deep learning models have been developed to identify and detect instruments and anatomical structures in surgical videos, these models are typically trained on manually labeled, procedure- and task-specific datasets that are relatively small, results in limited generalization capability to unseen data. In fact, a massive amount of raw surgical data, including videos captured during various surgical procedures everyday in hospitals. Given that labeling all of this raw surgical data is nearly impractical due to the need for highly specialized expertise, recent success of vision-language models (VLMs) - which can be trained on large volumes of raw image-text pairs and gain strong adaptability - offers a promising alternative for leveraging raw surgical data. While a few studies have begun exploring VLMs for surgical data, their performance remains limited. To support future development of more effective VLMs for surgical applications, this paper aims to answer a key question: *How well do existing VLMs - both general-purpose and surgery-specific - perform on surgical data, and what type of scenes do they struggle with?* Therefore, we conduct a benchmarking study of several popular VLMs across diverse datasets of gastrointestinal surgery and general surgery. Specifically, we visualize the model's attention to identify which regions of the image it focuses on when making predictions for surgical tasks. We also propose several metrics to evaluate whether the model attends to task-relevant regions. Our findings reveal a mismatch between prediction accuracy and visual grounding.

1 Introduction

Minimally invasive surgery (MIS) enables procedures to be performed through small incisions, offering substantial benefits for patients such as reduced bleeding and pain, and faster recovery times. However, MIS also brings many challenges for surgeons including the limited field-of-view and reduced depth perception from the endoscope, which is a small camera inserted into the patient body to provide visualization of the surgical site, affecting surgeons' hand-eye coordination ability [1]. To reduce unintended damage and enhance patient outcomes, many studies have proposed machine learning (ML) and deep learning (DL) models to analyze surgical videos, with the goal of providing real-time guidance and informing potential risks to surgeons during procedures. These models have been applied to tasks such as surgical tool and tissue classification, semantic and instance segmentation, phase and action recognition, workflow analysis, and surgical skill assessment [2, 3, 4]. Despite these efforts, most existing models in this field remain task-specific and were trained using relatively small datasets, usually consisting of thousands of images manually annotated by clinical experts. However, due to visual challenges inherent in surgical scenes, such as varying lighting conditions, textureless and moist tissues, occlusions, motion blur, and the presence of blood and smoke, these datasets are often insufficient for models to generalize effectively to unseen videos, even within the same type of procedure.

Although manual annotation of surgical data is difficult to scale, if a model can tolerate low-quality labels, there actually exists a massive amount of raw surgical data that can be leveraged. For example, since surgeons cannot view the surgical site directly as in traditional open surgeries, MIS has been routinely performed under video guidance. As a result,

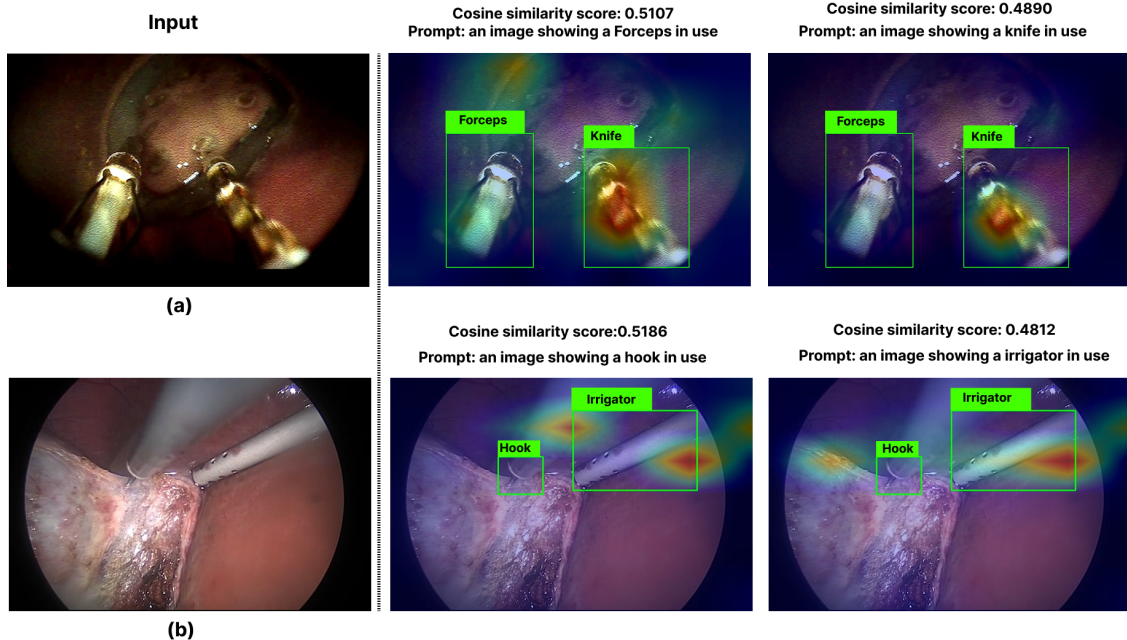


Figure 1: Examples of a VLM, CLIP-ViT-B/32, performing surgical instrument classification. The first column shows two input images. The next two columns show the classification results from the VLM and the corresponding model attention maps generated by Grad-CAM. We report the cosine similarity scores estimated by the VLM for the top two classes with highest cosine similarity scores. Green bounding boxes overlaid on the attention maps are ground truth annotations, (a) from the CoPESD dataset [11] and (b) from the CholecT80-BBox dataset [10] both show that VLMs may not consistently focus on the most relevant locations.

large volumes of surgical video data are generated every day, much of which is already stored in hospital databases. Additionally, numerous instructional videos and educational resources for medical education are publicly available online. If we can develop a model capable of efficiently learning from such large-scale raw surgical data, it may achieve a level of generalization that is hard to reach using existing ML/DL models for surgical applications trained on much smaller datasets. Models like CLIP [5] learn visual-text representations using contrastive learning, a technique that encourages the model to bring representations of paired images and text closer together in a multi-modal embedding space, while pushing apart representations of mismatched pairs. This approach reduced the need for meticulously labeled datasets by leveraging weak supervision from natural correspondences between images and their descriptions. The success of VLMs points out a promising way to use large volumes of raw surgical data.

Recent efforts in surgical AI have begun to explore the development of foundation models for surgical environments [35]. SurgVLP, HecVL, and Peskavlp[9, 8, 7] are trained using contrastive learning on surgical videos paired with text, with each method adding progressively more structure or supervision to improve alignment. Moreover, surgical data exhibits a long-tailed distribution, with many rare yet complex cases appearing only occasionally during procedures [29, 31]. As a result, even models with strong generalization ability, including such as VLMs, can still fail in these less-represented scenarios.

In surgery, a single misjudgment can lead to serious complications like excessive bleeding, organ damage, or even life-threatening outcomes. Therefore, it is crucial to detect when a model may fail so that clinicians are aware of the limitations of this model and know when to rely more on their own expertise to make a decision. Explainability in AI is an evolving field focused on interpreting model predictions and understanding when and how the model fails. Explainability requires the model not only to make accurate prediction but also to ground its reasoning on the most relevant cues. Given the high-stakes nature of surgical applications, incorporating explainability into these models is essential for ensuring informed clinical decision-making. Recently, there has been growing interest in providing explanations for neural networks to better understand their transparency and credibility [12, 21, 24, 20, 30]. In particular, recent work [12] highlights a key concern in VLMs: they often attend to irrelevant background regions rather than task-relevant objects, raising concerns about models making correct predictions for the wrong reasons, which undermines their reliability and interoperability. In this work, we adopt existing explainability techniques to study the reliability and interpretability of VLMs in surgical settings. Specifically, we incorporate CAM methods such as Grad-CAM [14] to

visualize the spatial regions that contribute most to a model’s prediction. These heatmaps allow us to assess whether the model’s attention aligns with the relevant surgical content, as illustrated in Figure 1.

Given that the application of VLMs in surgical environments is still in its early stages, and considering the diversity of available VLM architectures, training strategies, and the substantial resources required for data collection, curation, model training, a benchmarking study is needed to evaluate the performance and limitations of existing VLMs and to guide future development of surgical VLMs. To the best of our knowledge, only one prior work by Rau et al. [13] has conducted a comprehensive benchmark of VLMs in the surgical domain, evaluating 11 state-of-the-art VLMs across 17 core surgical visual understanding tasks, including classification, detection, segmentation, and risk assessment. Their results indicate that while current VLMs demonstrate strong generalization abilities, their performance remains far below the accuracy required for practical application in surgical tasks. However, their evaluation focuses primarily on standard metrics such as F1 score, revealing only the average performance across datasets, which may not provide sufficient insight for determining effective surgical VLM training strategies. Therefore, in this work, we adopt an existing neural network explainability technique CAM to analyze which image regions have greater impact on the model’s decision-making process, thereby providing better guidance for future development of surgical VLMs. In this work, we benchmark pre-trained VLMs on tasks involving surgical scene understanding, with a focus on their zero-shot interpretability and spatial alignment. Our main contributions are as follows:

- We introduce a VLM benchmarking framework for surgical data that goes beyond standard evaluation workflows by incorporating model explainability. We visualize attention maps to reveal which regions of an image have the greatest influence on the model’s predictions.
- We propose several new metrics to quantitatively analyze the attention maps and evaluate the reliability of VLM predictions. These metrics complement standard metrics and enable a more comprehensive evaluation of the models

2 Related Work

2.1 VLM

VLMs have established a powerful paradigm for bridging visual and textual modalities. A prominent example is CLIP [5], which learns visual-text representations through contrastive learning using an image encoder (e.g., ResNet [33] or Vision Transformer [32]) and a text encoder that learn a joint embedding space by aligning images and natural language descriptions during training on large-scale image-text pairs from the web. This approach leverages available web data without requiring manual annotations, demonstrating how models can learn meaningful representations directly from raw, unstructured data sources. At inference time, CLIP takes an image and a set of natural language prompts (e.g., “a photo of a grasper” or “an image showing surgical scissors”) and computes the similarity between the image embedding and each text embedding to determine the most relevant match. The effectiveness of CLIP-style VLMs heavily depend on how well the text prompts align semantically and structurally with the image content, which ideally should imply that the VLM can focus on the correct regions of the image that correspond to the described concepts.

2.2 VLM for surgical applications

Recent efforts on VLMs for surgical applications have explored using training data from both narrated surgical videos and slide-guided surgical lectures to enhance the models’ generalization capabilities. SurgVLP [9] introduced a large-scale surgical pretraining approach using data from surgical lecture videos. It adopts a CLIP-style training paradigm with a contrastive learning objective to align video clips and textual descriptions in a shared embedding space. A follow-up model, HecVL [8], enhances this framework by introducing hierarchical supervision, pairing videos with both free-form text and structured phase- and procedure-level annotations, leading to improved phase recognition. PeskaVLP [7] further extends this line of work by incorporating LLM-augmented surgical knowledge into the texts and applying a procedure-aware loss to improve cross-modal temporal alignment. Other foundation model such as GSViT[36], trained on 680 hours of surgical videos that learns to predict what happens next in surgery videos, and is fast enough to analyze surgical footage in real-time to potentially assist surgeons or control surgical robots during live operations. Learning from a large number of surgical videos and lectures allows surgical VLMs to have the ability to recognize surgical phases and identify the actions performed in different video clips. In this work, we also evaluate these models’ performance on more detailed object-level understanding, such as recognizing tissues and instruments.

2.3 Visual explanation methods for Deep learning

While deep learning enable superior performance, their lack of decomposability into intuitive and understandable components makes them hard to interpret. Consequently, when today’s intelligent systems fail, they fail without warning or explanation, producing outputs that cannot always be trusted. To mitigate this challenge, several methods have been developed to visualize which regions of an image have the most influence on model predictions, with the goal of revealing the evidence the model relies on to make its predictions, thereby providing insight into their explainability. Grad-CAM [14] highlights important regions by computing the gradients of the output with respect to intermediate feature maps of convolutional networks, and demonstrates its usefulness in helping users build appropriate trust in model predictions. Recent work [20] extends this idea by computing gradients with respect to attention layers. Other works such as, Grad-CAM++ [21] refines the original approach by improving localization in cases with multiple object instances, using a weighted average of higher-order derivatives. Score-CAM [22], on the other hand, avoids gradient computation altogether by using the model’s output scores to directly weight the activation maps. This can lead to more stable results, though at a higher computational cost. In our work, we adapt the original Grad-CAM method due to its simplicity and ease of implementation, and use it as one core tool in our benchmark.

2.4 Evaluation metrics for Surgical data

To the best of our knowledge, Rau et al. [13] is the only prior work that conduct benchmarking of VLMs on surgical data. It evaluates several commonly studied tasks such as instrument and anatomy classification, segmentation, and the identification of risk- or safety-related information, using standard evaluation metrics like the F1 score. Recently, there are studies highlights the need for new metrics to complement standard evaluation methods by capturing aspects of model performance that traditional metrics may overlook [23]. Given that our paper focuses on analyzing model attention, we propose several new metrics to assess the extent to which the model’s predictions rely on correct attention. These metrics are inspired by several prior studies that analyze attention maps to gain insight into model behavior. For spatial semantic grounding, Chen et al. [24] introduce the use of IoU to evaluate gScoreCAM by measuring the overlap between binarized attention maps and ground-truth object regions. However, this approach overlooks the varying strength of contribution across different regions—an important factor in surgical images due to their complex visual scenes. Furthermore, when the model’s prediction is incorrect, its attention is often misaligned, making it difficult to assess whether the attention mechanism is meaningful or trustworthy. Choe et al. [37] propose the *Localization Accuracy* metric for weakly supervised object localization, which considers a prediction correct only when both the predicted class label and the localized region (from a saliency map) align with the ground truth. It evaluate not only attending to the correct region but also predicting the correct semantic label.

3 Proposed Methods

In this section, we first introduce the visual tasks for understanding surgical images in Section 3.1 and problem evaluated in this benchmark in Section 3.2. We then describe the Class Activation Mapping (CAM) techniques, including methods designed for ResNet-based architectures as well as those adapted for transformer-based models in Section 3.3. Finally, we describe the metrics used to evaluate the VLMs, including standard task metrics as well as newly proposed metrics for analyzing attention maps, as described in section 3.4.

3.1 Task Definition

Our study focuses on two key tasks: (i) *instrument classification and grounding* and (ii) *surgical action classification via triplet descriptions*.

Instrument Classification Task: In the instrument classification task, a VLM selects the most semantically aligned description from a pool of prompts, each referring to a specific surgical instrument class.

Triplet Classification Task: In the triplet classification task [34], a VLM is evaluated on its ability to infer structured surgical actions represented as subject-action-object triplets, where the subject denotes the surgical instrument (e.g., grasper), the action refers to the surgical motion (e.g., retract), and the object indicates the anatomical target (e.g., gallbladder).

3.2 Problem Definition

In addition to benchmarking the performance of VLMs on surgical data, a main objective of this work is to assess whether their predictions are grounded in the correct visual evidence. Formally, this motivates the following question:

- **When the model makes a correct prediction**, does its attention focus on the relevant regions in the image that support that decision?
- **When the model makes an incorrect prediction**, is it attending to the wrong visual cues?

By examining these two scenarios, we aim to better understand not just *what* the model predicts, but *why*—providing insight into its reasoning process and the reliability of its visual grounding. Answering this requires going beyond classification accuracy and assessing whether the model’s visual focus meaningfully supports its predictions. To do so, we introduce visualization-based methods in the next section.

3.3 Class Activation Mapping

Class Activation Mapping (CAM) methods aim to localize the regions in an image that contribute to a model’s decision. These methods work by analyzing the internal activations of a convolutional neural network and their influence on a target output score. Here, we provide a brief explanation of how Grad-CAM works in two commonly used visual encoders of VLMs: ResNet[33] and Visual Transformer[32].

3.3.1 Grad-CAM for ResNet VLM

For VLMs that use ResNet-style backbones [9, 8, 7], the Grad-CAM formulation is defined as follows. Let $I \in \mathbb{R}^{H' \times W' \times 3}$ be the input image, and let $A \in \mathbb{R}^{K \times H \times W}$ denote the output of a selected convolutional layer in the image encoder, where K is the number of channels and $H \times W$ is the spatial resolution. Let $A_k(i, j)$ denote the activation at spatial position (i, j) in channel k . Let $\mathcal{P} = \{P_1, P_2, \dots, P_N\}$ be a set contain N candidate natural language prompts. The vision-language model computes an embedding for the image $\phi_{\text{img}}(I)$ and for each text prompt $\phi_{\text{text}}(P_k)$, and calculates a similarity score S_{P_k} (typically cosine similarity) for each prompt in \mathcal{P} :

$$S_{P_k} = \frac{\phi_{\text{img}}(I)^\top \phi_{\text{text}}(P_k)}{\|\phi_{\text{img}}(I)\| \cdot \|\phi_{\text{text}}(P_k)\|}.$$

The predicted prompt \hat{T} is then selected as the one with the highest similarity score:

$$\hat{P} = \arg \max_{P_k \in \mathcal{P}} S_{P_k},$$

and let $S_{\hat{T}}$ denote the scalar similarity score corresponding to the predicted prompt \hat{T} . Grad-CAM computes the gradient of the score S_c with respect to the feature map $A_k(i, j)$, and then applies global average pooling over spatial dimension:

$$\alpha_k = \frac{1}{H \cdot W} \sum_{i=1}^H \sum_{j=1}^W \frac{\partial S_{\hat{P}}}{\partial A_k(i, j)}.$$

The gradient tells how much each feature map channel A_k contributes to the model’s prediction $S_{\hat{c}}$. it does this by averaging the gradient of predicted score with respect to all locations (i, j) in that channel and use it act as a weight that reflects the importance of that channel. Based on it, to compute the Grad-CAM heatmap, we first obtain a weighted combination of the activation maps using channel-wise importance weights α_k , followed by a ReLU non-linearity. Finally, we apply bilinearly upsampling to resize L to the size of original image.

$$L_{\text{Grad-CAM}} = \text{Upsample}_{\text{bilinear}} \left(\text{ReLU} \left(\sum_{k=1}^K \alpha_k \cdot A_k \right) \right). \quad (1)$$

3.3.2 Gradient-Based Attention Rollout for CLIP-ViT

Grad-CAM can be adapted to CLIP-ViT, specifically CLIP [5] with a ViT image encoder. Following the method from [20], instead of using convolutional feature maps, we leverage the self-attention matrices and their gradients to identify input image patches that contribute most to the similarity between an image and a given text prompt. Let $\mathcal{T}^{(l)} \in \mathbb{R}^{N \times N}$ denote the self-attention matrix from the l -th transformer block in the ViT encoder, where N is the number of tokens, including the [CLS] token, a special token added at the beginning of the input, and its output representation is used to summarize the entire image for classification tasks. We extract $\mathcal{T}^{(l)}$ after the softmax operation during the forward pass.

We compute the gradient of the similarity score with respect to the attention map:

$$\nabla \mathcal{T}^{(l)} = \frac{\partial S_{\hat{P}}}{\partial \mathcal{T}^{(l)}},$$

where $S_{\hat{T}}$ is the predicted similarity score corresponding to the selected text prompt in a zero-shot setting. To capture influence on the similarity score, we compute the gradient-weighted attention map:

$$\tilde{\mathcal{T}}^{(l)} = \text{ReLU} \left(\nabla \mathcal{T}^{(l)} \odot \mathcal{T}^{(l)} \right),$$

where \odot denotes the elementwise (Hadamard) product. This highlights token-to-token interactions that both receive high attention and significantly impact the similarity score. To propagate relevance through the transformer layers, we recursively update a relevance matrix $\mathbf{R}^{(l)} \in \mathbb{R}^{N \times N}$ as follows:

$$\mathbf{R}^{(L)} = I, \quad \mathbf{R}^{(l)} = \mathbf{R}^{(l+1)} + \tilde{\mathcal{T}}^{(l)} \mathbf{R}^{(l+1)},$$

starting from the final layer L , where I is the $N \times N$ identity matrix. This recursive formulation accumulates relevance flow across all layers. Let each patch token indexed by $k \in \{1, \dots, N-1\}$, after propagating to the input layer, we extract the relevance scores from the [CLS] token to each image patch token:

$$r_k = \mathbf{R}_{\text{CLS}, k}^{(0)}, \quad \text{for } k = 1, \dots, N-1,$$

where r_k denotes the relevance of the k -th image patch token to the final similarity score.

Finally, we reshape and upsample the vector $[r_1, \dots, r_{N-1}] \in \mathbb{R}^{N-1}$ into the input image size using bilinear interpolation. The final heatmap can be constructed as following:

$$L_{\text{Grad-CAM-ViT}} = \text{Upsample}_{\text{bilinear}} \left(\text{reshape}([r_1, \dots, r_{N-1}]) \right), \quad (2)$$

3.4 Evaluation Metrics

Inspired by [37], we adopt a similar class-aware localization metric in our work to assess vision-language models in surgical settings. In this section, we introduce the metrics for instruments and triplet classification tasks.

3.4.1 Instrument classification metrics

Conventional evaluation for this task in [13] treats it as a multi-label classification problem and reports the F1 score by thresholding the image-text similarity score for each instrument class, selecting the optimal threshold per class, and averaging F1 scores across all instruments.

We now introduce our metrics, let I denote an input image of size $H \times W$, and let T be a corresponding text prompt. The model produces a Grad-CAM heatmap $L(i, j) \in \mathbb{R}^{H \times W}$ using (1) or (2), where each pixel (i, j) reflects the spatial importance of that location for the model’s prediction. We normalize L to the range $[0, 1]$, and apply a fixed threshold $\tau \in [0, 1]$ to obtain information about the "strength" of different regions. We now define the predicted τ -attention region as following:

$$\mathcal{A}_\tau = \{(i, j) \in \{1, \dots, H\} \times \{1, \dots, W\} \mid L(i, j) \geq \tau\}.$$

Let $\mathcal{C} = \{c_1, \dots, c_K\}$ denote the set of ground-truth class labels (e.g., surgical instruments) present in the image. In Section 4, we will explain how these classes are used to construct prompts for VLMs using predefined templates. For each class $c_k \in \mathcal{C}$, let $\mathcal{G}_{c_k}^{(r)} \subseteq \{1, \dots, H\} \times \{1, \dots, W\}$ denote the set of pixel coordinates in the r^{th} annotated region of class c_k , for $r = 1, \dots, N_k$. Let \hat{c} be the class predicted by the model. We define the set of all annotated pixels (regardless of class) as:

$$\mathcal{G}_{\text{all}} = \bigcup_{k=1}^K \bigcup_{r=1}^{N_k} \mathcal{G}_{c_k}^{(r)} \subseteq \{1, \dots, H\} \times \{1, \dots, W\}.$$

We define the set of pixels corresponding to the predicted class \hat{c} as:

$$\mathcal{G}_{\hat{c}} = \begin{cases} \bigcup_{c_k = \hat{c}} \bigcup_{r=1}^{N_k} \mathcal{G}_{c_k}^{(r)}, & \text{if } \hat{c} \in \mathcal{C} \\ \emptyset, & \text{otherwise} \end{cases}$$

(1) Thresholded Attention Coverage (τ -AC):

This metric measures how much of the model’s attention region overlaps with any annotated object, regardless of class correctness:

$$\tau\text{-AC} = \frac{|\mathcal{A}_\tau \cap \mathcal{G}_{\text{all}}|}{|\mathcal{A}_\tau|}. \quad (3)$$

It reflects the fraction of model attention that lands inside any annotated region. This is a less strict metric that serve as a soft proxy to access whether the model is at least focusing on some semantically meaningful area.

(2) Thresholded Attention Alignment (τ -AA):

This metric evaluates whether the model’s attention aligns specifically with the annotated regions of the predicted class \hat{c} . If $\hat{c} \notin \mathcal{C}$, the score is defined to be zero:

$$\tau\text{-AA} = \begin{cases} \frac{|\mathcal{A}_\tau \cap \mathcal{G}_{\hat{c}}|}{|\mathcal{A}_\tau|}, & \text{if } \hat{c} \in \mathcal{C} \\ 0, & \text{otherwise} \end{cases} \quad (4)$$

This ensures that only alignment with correctly predicted classes contributes positively to the score. Beyond conventional classification tasks, understanding the surgical action depicted in an image is also critically important in surgical data. In the instrument classification task, models are not required to predict all classes present in the image. Instead, we generate the heatmap L_{GradCAM} and $L_{\text{GradCAM-VIT}}$ and evaluate spatial grounding using two metrics: τ -AC, which assesses whether the model attends to any relevant region, and τ -AA, which evaluates whether attention is correctly aligned with the specific object mentioned in the prompt.

3.4.2 Standard Triplet evaluation metrics

(1) Triplet Classification: To evaluate the performance of vision-language models (VLMs) on surgical action recognition, we adopt conventional classification metrics based on the triplet recognition task introduced in [34]. Each predicted action is represented as a triplet of class labels $\langle \text{instrument, verb, target} \rangle = (s, v, o)$, corresponding to the subject (surgical instrument), verb (action), and object (anatomical target), respectively. Given a ground-truth triplet (s^*, v^*, o^*) and a predicted triplet (s, v, o) , we define binary match indicators for each component as follows:

$$\text{TripletMatch}(s, v, o; s^*, v^*, o^*) = (\mathbb{1}_{s=s^*}, \mathbb{1}_{v=v^*}, \mathbb{1}_{o=o^*}) \quad (5)$$

We now formally define the following conventional evaluation metrics we mentioned in section 3.1:

IVT Accuracy (Full Triplet Accuracy): $\text{IVT} = \mathbb{1}_{(s,v,o)=(s^*,v^*,o^*)}$

IV Accuracy (Instrument-Verb Accuracy): $\text{IV} = \mathbb{1}_{(s,v)=(s^*,v^*)}$

IT Accuracy (Instrument-Target Accuracy): $\text{IT} = \mathbb{1}_{(s,o)=(s^*,o^*)}$

These combinations are evaluated because surgical actions are inherently instrument-centric; both the verb and target gain semantic meaning only when grounded in the context of the instrument performing the action.

(2) Action Reasoning Score (ARS): In the triplet classification task, the traditional and straightforward way of evaluating performance is to compute the F1 classification score for each class. However, in this paper, beyond assessing classification accuracy, we also challenge the spatial reasoning ability of VLMs. However, when it comes to localizing the bounding box of an action verb, the problem becomes more complex. As discussed in [25], the localization of the action region is closely related to the instrument performing the action. In particular, when an instrument is actively performing an action, the action is spatially grounded near the location of the instrument tip. Due to the lack of labeled action verb bounding boxes, we propose the **Action Reasoning Score (ARS)**, it measures whether the model’s attention for a predicted action (verb) overlaps with the bounding box of the predicted instrument (subject). Let a predicted triplet be denoted by (s, v, o) , where $s \in \mathcal{S}$ is the subject, $v \in \mathcal{V}$ is the verb (e.g., an action such as *cut*), and $o \in \mathcal{O}$ is the object (e.g., *tissue*) and ground-truth triplet is (s^*, v^*, o^*) . We compute ARS **only when**: $s = s^*$ and $v = v^*$. Let the image be defined over a pixel grid of height H and width W , with each pixel indexed by coordinates $(i, j) \in \{1, \dots, H\} \times \{1, \dots, W\}$. Let $L_v(i, j) \in [0, 1]$ denote the value of Grad-CAM attention produced by (1) or (2) at pixel (i, j) for the predicted verb v . We will later show how to generate the attention heatmap L_v and construct prompts using predefined templates for VLMs in section 4.

For a fixed threshold $\tau \in [0, 1]$, we define the τ -attention region for verb as following:

$$\mathcal{A}_{\tau v} = \{(i, j) \mid L_v(i, j) > \tau\}.$$

Recall that $\mathcal{B}_s \subseteq \{1, \dots, H\} \times \{1, \dots, W\}$ denote the set of pixels within the bounding box of the predicted instrument s . We define the *Action Reasoning Score (ARS)* as:

$$\text{ARS}(s, v) = \begin{cases} \frac{|\mathcal{A}_{\tau v} \cap \mathcal{B}_s|}{|\mathcal{A}_{\tau v}|}, & \text{if } s = s^*, v = v^* \\ 0, & \text{otherwise} \end{cases} \quad (6)$$

Note that this score provides a soft measure of how much the verb-specific attention overlaps with the instrument’s spatial region, offering insight into whether the model is focusing on a plausible area for grounding the action. While there is no strict threshold for overlapping, a higher value generally indicates better spatial alignment, whereas a near-zero value suggests the model is likely attending to an irrelevant region.

4 Experiments Set up

All experiments use a fixed Grad-CAM threshold of $\tau = 0.3$ to generate attention maps for grounding evaluation. We first introduce the prompt designs used across all tasks, followed by a description of the benchmarked models evaluated in this work. We evaluate our methods using three surgical video datasets. The Cholec80-BBox dataset [26, 27], which extends the original Cholec80 dataset [10], consists of five laparoscopic cholecystectomy videos with instrument bounding box annotations and is used for instrument classification. The CoPESD dataset [11] includes two endoscopic submucosal dissection procedures with two type of tool annotations and is also used for instrument classification. The CholecT45 dataset [28] comprises 45 laparoscopic cholecystectomy videos annotated with action triplets and instrument bounding boxes, and is used for evaluating both triplet classification and action reasoning.

Prompt Design and Evaluation Strategy: To align with the prompt-based input format of VLMs, we construct a pool of prompts using template-based formulations. For instrument classification, we use prompts template: “*an image showing a {instrument class} in use*”, covering all possible instrument classes in Cholec80. For triplet-based action reasoning, we use the template “*I use a {instrument} to {verb} the {target}*”.

For triplet reasoning, we compute the **Action Reasoning Score (ARS)** is computed only for cases where $IV = 1$, that is, both the subject (instrument) and verb predictions are correct. In our implementation, similar to the instrument classification setup, we first generate a pool of triplet prompts using the template “*I use a {instrument} to {verb} the {target}*”, covering all possible instrument, verb, and target classes. We then identify frames where both the predicted instrument and verb match the ground truth. For these correctly classified frames, we reuse the predicted verb to construct a secondary prompt of the form “*I am performing {predicted_verb}*”. Finally, we generate its Grad-CAM heatmap L_v and compute the action reasoning scores (6).

Due to all datasets used in this study are not yet fully released, we leverage all available video folders and conduct experiments on all released portions.

4.1 Benchmarked Models

In this work, we evaluate four VLMs: CLIP-ViT[5], HecVL[8], PeskaVLP[7], and SurgVLP[9]. CLIP-ViT [5] is the classic and widely adopted architecture for multi-modal learning, trained on large-scale natural image-text pairs. CLIP has demonstrated strong zero-shot performance across various domains, making it a natural reference point for evaluating domain transfer to surgical imagery.

The other three models: SurgVLP, PeskaVLP, and HecVL are trained using surgical video datasets with varying levels of supervision, and architectural adaptations. These models are designed specifically to address the challenges of understanding visual-linguistic information in surgical environments, such as tool usage, procedural context, and anatomy. We aim to assess not only a deeper understanding of the reasoning capabilities of VLMs in surgical classification tasks, but also the limitations and trade-offs between general-purpose and task-specific VLMs within the current surgical domain.

5 Results

5.1 Instrument Classification Performance

We first report the thresholded attention coverage (τ -AC) and thresholded attention alignment (τ -AA) scores of instrument classification tasks, τ -AC quantifies the proportion of model attention that overlaps with any annotated tool region. τ -AA further restricts the evaluation to the tool class predicted by the model.

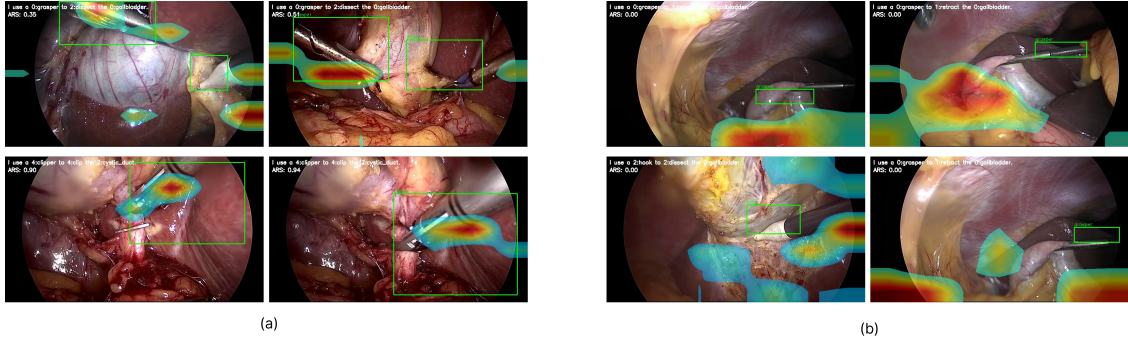


Figure 2: Examples of triplet classification tasks using CLIP-ViT with Grad-CAM visualize the verb heatmap L_v , where CLIP-ViT successfully classifies all images in Panels (a) and (b) with the correct instrument and verb. Green bounding boxes indicate ground truth annotation from video 42 and 43 in CholecT80-BBox dataset. Panels (a) illustrate Ideal action reasoning, with attention focused near the instrument and high ARS scores. In contrast, panels (b) show failure cases: despite correct triplet predictions, the attention is misplaced on background tissues, leading to ARS scores of 0.00. These examples highlight that some correct classifications are not based on the correct spatial evidences.

Model	Video-41		Video-42		Video-43		Video-44		Video-45		CoPESD	
	τ -AC	τ -AA										
CLIP-ViT	0.2022	0.0356	0.2483	0.0893	0.2926	0.0445	0.2038	0.0484	0.2395	0.1021	0.3405	0.0680
HecVL	0.0574	0.0097	0.0953	0.0334	0.0824	0.0199	0.0503	0.0162	0.0565	0.0285	0.1586	0.0653
PeskaVLP	0.0918	0.0333	0.1301	0.0373	0.1252	0.0341	0.1030	0.0306	0.1225	0.0637	0.2145	0.0714
SurgVLP	0.0659	0.0111	0.0917	0.0164	0.1215	0.0275	0.0736	0.0118	0.0645	0.0203	0.2247	0.1522

Table 1: Spatial grounding performance for instrument classification per video folder (video-41 to video-45) in the Cholec8k Bounding Box dataset, and overall on CoPESD at threshold $\tau = 0.3$. Each cell contains either Attention Correctness (τ -AC) or Attention Agreement (τ -AA).

Table 1 shows the spatial reasoning performance of five vision-language models across two datasets. Overall, all VLMs tested so far struggle under complex surgical environments. CLIP achieves the highest scores on the CoPESD dataset, which contains fewer visible instrument instances. It consistently outperforms the other models in both τ -AC and τ -AA metrics across most videos, achieving a τ -AC of 0.3405 and τ -AA of 0.0680 on the CoPESD dataset, and a τ -AC of 0.2395 and τ -AA of 0.1021 on the Cholec8k Bounding Box dataset. In contrast, despite being trained on surgical lectures, HecVL, PeskaVLP, and SurgVLP perform worse compared to the general-purpose model CLIP. We hypothesize that this is because these models are primarily designed to understand high-level surgical phases rather than to perform fine-grained, frame-level instrument classification. Overall, while VLMs demonstrate some ability to localize surgical instruments, they still lack the capacity to consistently and correctly classify them in challenging surgical scenes.

5.2 Triplet Classification

We compute the Action Reasoning Score (ARS), which evaluates whether the attention map for a predicted action verb overlaps with the correct instrument’s spatial location. This requires datasets that provide both triplet-level annotations and bounding box supervision. We combine the CholecT45 dataset (triplet annotations) and the Cholec80BoundingBox dataset (bounding boxes); only two video folders—**video-42** and **video-43** are common to both.

Video	SurgVLP			PeskaVLP			HecVL			CLIP-ViT		
	ARS	V/T (%)	Z/V (%)	ARS	V/T (%)	Z/V (%)	ARS	V/T (%)	Z/V (%)	ARS	V/T (%)	Z/V (%)
Video-42	0.0669	30.5	59.1	0.0744	50.9	43.4	0.0736	68.1	46.9	0.0895	24.2	20.6
Video-43	0.0535	19.7	53.0	0.0673	24.1	51.1	0.0832	24.3	45.9	0.1486	9.5	19.2

Table 2: Action Reasoning Score (ARS) and evaluation coverage for each model on CholecT45 videos **42** and **43**, using bounding boxes from Cholec80. Each model reports: ARS at threshold $\tau = 0.3$; V/T is the percentage of valid frames, defined as the proportion of frames where both the instrument and verb are correctly predicted. Let T denote the total number of frames in the video folder, then $V/T = \frac{1}{T} \sum_{i=1}^T \mathbb{1}_{(s_i=s_i^*) \wedge (v_i=v_i^*)}$ Z/V is the percentage of those valid frames that receive zero ARS.

Based on Table 2, CLIP-ViT shows a better ability to pay attention to the right location when reasoning about the action verb. For example, it achieves the highest ARS scores among all models, with **0.0895** on Video-42 and **0.1486** on Video-43. However, it struggles to classify surgical instruments accurately, as shown by its low valid prediction rates: only **24.2%** of frames in Video-42 and **9.5%** in Video-43 have both the instrument and verb correct. On the other hand, SurgVLP, PeskaVLP, and HecVL show lower ARS scores (e.g., SurgVLP: **0.0669** on Video-42 and **0.0535** on Video-43) but relatively higher classification accuracy, with HecVL achieving valid frame rates of **68.1%** and **24.3%** on Videos 42 and 43, respectively. However, among these valid predictions, a large portion have zero ARS scores — for instance, **59.1%** of valid frames in SurgVLP (Video-42) and **53.0%** in Video-43 show no spatial alignment with the action verb.

5.3 Discussion

Based on the results, we observe that the overall performance of VLMs on surgical data is generally limited. For CLIP, we observed that it can focus on the correct object and achieves relatively good ARS scores for the verb associated with the instrument. This suggests that VLMtrained on diverse, large-scale datasets can still perform relatively well on downstream tasks, leveraging their generalized understanding from broad visual concepts. However, we also observed a notable gap between classification accuracy and ARS scores, indicating that the models often make correct predictions without actually attending to the correct spatial regions.

Another problem is the discrepancy between classification and attention, for SurgVLP, PeskaVLP, and HecVL. We believe the main issues is that those three models are trained to focus more on the high-level structure of surgical videos. As a result, they may rely heavily on phase-level patterns and struggle to capture fine-grained, frame-level details. These models often learn from broader contextual cues such as surgical summaries or accompanying audio rather than detailed spatial features within individual frames. This reliance on high-level context means they may overlook the specific regions relevant to the text prompt. We provide Figure 2 to visually illustrate this issue and make the spatial misalignment more evident.

6 Conclusion

Our work introduces a benchmarking framework for evaluating VLMs in surgical settings, with a focus on spatial attention and grounding beyond standard accuracy metrics. We propose new evaluation measures that assess how well model attention aligns with corresponding relevant regions, providing deeper insight into model behavior. Our findings reveal not only the generally low performance of VLMs on surgical data, but also a consistent disconnect between correct predictions and appropriate visual focus. These issues raise critical concerns about the reliability and interpretability of current VLMs in surgical applications. Even models trained specifically on surgical data struggle when faced with frame-level, fine-grained tasks such as action recognition and instrument classification.

References

- [1] R. Bogdanova, P. Boulanger, and B. Zheng, “Depth perception of surgeons in minimally invasive surgery,” *Surgical Innovation*, vol. 23, no. 5, pp. 515–524, 2016.
- [2] Apolline Sauzéon Twinanda, Sherif Shehata, Didier Mutter, Jacques Marescaux, Michel de Mathelin, and Nicolas Padoy. Endonet: A deep architecture for recognition tasks on laparoscopic videos. *IEEE Transactions on Medical Imaging*, 36(1):86–97, 2016.
- [3] Yuxuan Jin, Qi Dou, Lequan Yu, Jing Qin, Chi-Wing Fu, and Pheng-Ann Heng. Temporal convolutional networks for real-time surgical phase recognition. In *Medical Image Computing and Computer-Assisted Intervention (MICCAI)*, pages 281–291. Springer, 2020.

- [4] Orestis Zisimopoulos, Elias Flouty, and Danaïl Stoyanov. Deepphase: Surgical phase recognition in cataracts videos. In *Medical Imaging with Deep Learning (MIDL)*, 2018.
- [5] Alec Radford, Jong Wook Kim, Chris Hallacy, Aditya Ramesh, Gabriel Goh, Sandhini Agarwal, Girish Sastry, Amanda Askell, Pamela Mishkin, Jack Clark, et al. Learning transferable visual models from natural language supervision. In *Proceedings of the 38th International Conference on Machine Learning (ICML)*. PMLR, 2021. URL <https://proceedings.mlr.press/v139/radford21a.html>.
- [6] Junnan Li, Dongxu Li, Caiming Xiong, and Steven CH Hoi. Blip: Bootstrapping language-image pre-training for unified vision-language understanding and generation. In *International Conference on Machine Learning (ICML)*. PMLR, 2022. URL <https://proceedings.mlr.press/v162/li22n.html>.
- [7] Kun Yuan, Vinkle Srivastav, Nassir Navab, and Nicolas Padoy. Procedure-aware surgical video-language pretraining with hierarchical knowledge augmentation. In *Proceedings of the 38th Conference on Neural Information Processing Systems (NeurIPS)*, 2024.
- [8] Kun Yuan, Vinkle Srivastav, Nassir Navab, and Nicolas Padoy. Hecvl: Hierarchical video-language pretraining for zero-shot surgical phase recognition. *arXiv preprint arXiv:2405.10075*, 2024. URL <https://arxiv.org/abs/2405.10075>.
- [9] Kun Yuan, Vinkle Srivastav, Tong Yu, Joël L. Lavanchy, Jacques Marescaux, Pietro Mascagni, Nassir Navab, and Nicolas Padoy. Learning multi-modal representations by watching hundreds of surgical video lectures. *arXiv preprint arXiv:2307.15220*, 2023. URL <https://arxiv.org/abs/2307.15220>.
- [10] A. P. Twinanda, S. Shehata, D. Mutter, J. Marescaux, M. De Mathelin, and N. Padoy. Endonet: a deep architecture for recognition tasks on laparoscopic videos. *IEEE Transactions on Medical Imaging*, 36(1):86–97, 2016.
- [11] Guankun Wang, Han Xiao, Huxin Gao, Renrui Zhang, Long Bai, Xiaoxiao Yang, Zhen Li, Hongsheng Li, and Hongliang Ren. Copesd: A multi-level surgical motion dataset for training large vision-language models to co-pilot endoscopic submucosal dissection. *arXiv preprint arXiv:2410.07540*, 2024.
- [12] Y. Li, H. Wang, Y. Duan, J. Zhang, and X. Li, “A closer look at the explainability of contrastive language-image pre-training,” *Pattern Recognition*, p. 111409, 2025.
- [13] Anita Rau, Mark Endo, Josiah Aklilu, Jaewoo Heo, Khaled Saab, Alberto Paderno, Jeffrey Jopling, F Christopher Holsinger, and Serena Yeung-Levy. Systematic evaluation of large vision-language models for surgical artificial intelligence. *arXiv preprint arXiv:2504.02799*, 2025.
- [14] Ramprasaath R Selvaraju, Michael Cogswell, Abhishek Das, Ramakrishna Vedantam, Devi Parikh, and Dhruv Batra. Grad-cam: Visual explanations from deep networks via gradient-based localization. In *Proceedings of the IEEE International Conference on Computer Vision (ICCV)*, pages 618–626, 2017.
- [15] Jean-Baptiste Alayrac, Jeff Donahue, Paul Luc, Antoine Miech, Ian Barr, Arthur Mensch, Kathryn Millican, Malcolm Reynolds, Sebastian Borgeaud, Andrew Brock, et al. Flamingo: a visual language model for few-shot learning. *arXiv preprint arXiv:2204.14198*, 2022.
- [16] Yifan Liu, Canwen Xu, Ziyang Yan, Xiang Lin, Xipeng Song, Zhiyuan Liu, and Maosong Sun. Pre-train prompt tune: Towards efficient foundation model tuning. *arXiv preprint arXiv:2302.12246*, 2023.
- [17] Kaiyang Zhou, Jingkang Yang, Chen Change Loy, and Ziwei Liu. Conditional prompt learning for vision-language models. In *Proceedings of the IEEE/CVF Conference on Computer Vision and Pattern Recognition*, pages 16816–16825, 2022.
- [18] Xiwen Chen, Wenhui Zhu, Peijie Qiu, Hao Wang, Huayu Li, Haiyu Wu, Aristeidis Sotiras, Yalin Wang, and Abolfazl Razi. Prompt-ot: An optimal transport regularization paradigm for knowledge preservation in vision-language model adaptation. *arXiv preprint arXiv:2503.08906*, 2025.
- [35] Samuel Schmidgall, Ji Woong Kim, Jeffrey Jopling, and Axel Krieger. General surgery vision transformer: A video pre-trained foundation model for general surgery. *arXiv preprint arXiv:2403.05949*, 2024.
- [20] Hila Chefer, Shir Gur, and Lior Wolf. Generic attention-model explainability for interpreting bi-modal and encoder-decoder transformers. In *Proceedings of the IEEE/CVF international conference on computer vision*, pages 397–406, 2021.
- [21] Aditya Chattopadhyay, Anirban Sarkar, Prantik Howlader, and Vineeth N Balasubramanian. Grad-cam++: Generalized gradient-based visual explanations for deep convolutional networks. In *2018 IEEE Winter Conference on Applications of Computer Vision (WACV)*, pages 839–847. IEEE, 2018.
- [22] Haofan Wang, Zifan Wang, Pengfei Zhao, Yanfeng Pei, Xiaoyu Wang, Alan L. Yuille, and Wei Shen. Scorecam: Score-weighted visual explanations for convolutional neural networks. In *Proceedings of the IEEE/CVF Conference on Computer Vision and Pattern Recognition Workshops*, pages 24–25, 2020.

- [23] Isabel Funke, Dominik Rivoir, and Stefanie Speidel. Metrics matter in surgical phase recognition. *arXiv preprint arXiv:2305.13961*, 2023.
- [24] Peijie Chen, Qi Li, Saad Biaz, Trung Bui, and Anh Nguyen. gscorecam: What objects is clip looking at? In *Proceedings of the Asian Conference on Computer Vision*, pages 1959–1975, 2022.
- [25] Arnaud Twinanda, Emre Aksan, Raphael Sznitman, Peter Wolf, Leo Gruendlinger, Christoph Jud, and Tiago da Costa. Cholect50: A benchmark for surgical action triplet recognition. *arXiv preprint arXiv:2204.05235*, 2022. URL <https://arxiv.org/abs/2204.05235>.
- [26] N. A. Jalal, T. A. Alshirbaji, P. D. Docherty, H. Arabian, T. Neumuth, and K. Möller. Surgical tool classification & localisation using attention and multi-feature fusion deep learning approach. *IFAC-PapersOnLine*, 56(2): 5626–5631, 2023.
- [27] T. Abdalbaki Alshirbaji, H. Arabian, N. A. Jalal, A. Battistel, P. D. Docherty, T. Neumuth, and K. Moeller. Cholec80-boxes: Bounding-box labeling data for surgical tools in cholecystectomy images, 2024. To be submitted.
- [28] Kun Yuan, Nassir Navab, Nicolas Padoy, et al. Procedure-aware surgical video-language pretraining with hierarchical knowledge augmentation. *Advances in Neural Information Processing Systems*, 37:122952–122983, 2024.
- [29] A. Zia, K. Bhattacharyya, X. Liu, M. Berniker, Z. Wang, R. Nespolo, S. Kondo, S. Kasai, K. Hirasawa, B. Liu, et al., “Surgical tool classification and localization: results and methods from the MICCAI 2022 SurgToolLoc challenge,” *arXiv preprint arXiv:2305.07152*, 2023.
- [30] X. Zhang, Y. Quan, C. Shen, X. Yuan, S. Yan, L. Xie, W. Wang, C. Gu, H. Tang, and J. Ye, “From redundancy to relevance: Information flow in VLMs across reasoning tasks,” *arXiv preprint arXiv:2406.06579*, 2024.
- [31] A. G. Roy, J. Ren, S. Azizi, A. Loh, V. Natarajan, B. Mustafa, N. Pawlowski, J. Freyberg, Y. Liu, Z. Beaver, et al., “Does your dermatology classifier know what it doesn’t know? Detecting the long-tail of unseen conditions,” *Medical Image Analysis*, vol. 75, p. 102274, 2022.
- [32] A. Dosovitskiy, L. Beyer, A. Kolesnikov, D. Weissenborn, X. Zhai, T. Unterthiner, M. Dehghani, M. Minderer, G. Heigold, S. Gelly, J. Uszkoreit, and N. Houlsby, “An image is worth 16x16 words: Transformers for image recognition at scale,” in *International Conference on Learning Representations*, 2021.
- [33] K. He, X. Zhang, S. Ren, and J. Sun, “Deep residual learning for image recognition,” in *Proceedings of the IEEE Conference on Computer Vision and Pattern Recognition (CVPR)*, pp. 770–778, 2016.
- [34] C. I. Nwoye, T. Yu, C. Gonzalez, B. Seeliger, P. Mascagni, D. Mutter, J. Marescaux, and N. Padoy, “Rendezvous: Attention mechanisms for the recognition of surgical action triplets in endoscopic videos,” *Medical Image Analysis*, vol. 78, p. 102433, 2022.
- [35] Samuel Schmidgall, Ji Woong Kim, Alan Kuntz, Ahmed Ezzat Ghazi, and Axel Krieger. General-purpose foundation models for increased autonomy in robot-assisted surgery. *Nature Machine Intelligence*, pages 1–9, 2024.
- [36] Samuel Schmidgall, Ji Woong Kim, Jeffrey Jopling, and Axel Krieger. General surgery vision transformer: A video pre-trained foundation model for general surgery. *arXiv preprint arXiv:2403.05949*, 2024.
- [37] J. Choe, S. J. Oh, S. Lee, S. Chun, Z. Akata, and H. Shim, “Evaluating Weakly Supervised Object Localization Methods Right,” in *Proceedings of the IEEE/CVF Conference on Computer Vision and Pattern Recognition (CVPR)*, pp. 3133–3142, 2020.